Title
Close-Packed Nanowire-Bacteria Hybrids for Efficient Solar-Driven CO2 Fixation

Journal
Joule, 4(4)

ISSN
2542-4785

Authors
Su, Yude
Cestellos-Blanco, Stefano
Kim, Ji Min
et al.

Publication Date
2020-04-01

DOI
10.1016/j.joule.2020.03.001

Peer reviewed

Close-packed nanowire-bacteria hybrids for efficient solar-driven CO_2 fixation

Authors:

Yude Su[1†], Stefano Cestellos-Blanco[2†], Ji Min Kim[2†], Yue-xiao Shen[1], Qiao Kong[1], Dylan Lu[1, 3], Chong Liu[5], Hao Zhang[1], Yuhong Cao[1], Peidong Yang[1,2,3,4,6*]

Affiliations:

[1] Department of Chemistry, University of California, Berkeley, Berkeley, CA 94720, USA

[2] Department of Materials Science and Engineering, University of California, Berkeley, Berkeley, CA 94720, USA

[3] Materials Sciences Division, Lawrence Berkeley National Laboratory, Berkeley, CA 94720, USA

[4] Kavli Energy Nanosciences Institute, Berkeley, CA 94720, USA

[5] Department of Chemistry and Biochemistry, University of California, Los Angeles, Los Angeles, CA 90095, USA

[6] Lead Contact

[†] These authors contributed equally to this work.

[*] To whom correspondence should be addressed. Email: p_yang@berkeley.edu

Summary

Microbial electro- and photoelectrochemical CO_2 fixation, in which CO_2-reducing microorganisms are directly interfaced with a cathode material, represent promising approaches for sustainable fuel production. Although considerable efforts have been invested to optimize microorganism species and electrode materials, the microorganism-cathode interface has not been systematically studied. Here, investigation of the interface allowed us to optimize the CO_2-reducing rate of silicon nanowire/*Sporomusa ovata* system. Tuning the bulk electrolyte pH and increasing its buffering capacity supported the formation of a close-packed nanowire-bacteria cathode. Consequently, the resulting close-packed biohybrid achieved a CO_2-reducing current density of ~0.65 mA cm^{-2}. When coupled with a photovoltaic device, our system enabled solar-to-acetate production with ~3.6% efficiency over seven days.

Introduction

Interfacing living cells and inorganic materials has enabled the development of diverse technologies including but not limited to gene editing[1, 2], biosensing[3, 4] and microbial fuel cells[5, 6]. Notably, microorganisms have been introduced as "living" catalysts to the field of catalytic CO_2 fixation[7-13]. These microorganisms, principally chemoautotrophic bacteria, have metabolic pathways that can fix CO_2 into multi-carbon products[14]. Biohybrid CO_2-fixing systems, particularly those driven by renewable solar energy, represent a promising strategy for sustainable CO_2-to-chemical conversion[15]. The use of time-evolved living biocatalysts allows for high product selectivity, catalyst regeneration and long-term operation[16]. Remarkably, several of these microorganisms accept extracellular charge transfer and can be directly interfaced with a cathode to carry out CO_2 fixation[11-13]. Different strategies have been employed to improve the performance of these hybrid systems, such as optimization of electrode geometry[17], electrode surface engineering[18], bacteria adaptation[19, 20] and enrichment[21]. Particularly, our group has developed a photoactive and high-surface-area silicon (Si) nanowire electrode that allows for unassisted solar-to-chemical production when paired with acetogen *Sporomusa ovata* (*S. ovata*)[13]. The high surface area of the Si nanowire electrode[22] allows for greater bacteria-electrode interface and thus enhanced change transfer rate. However, the CO_2-reducing current of biohybrid systems mediated by direct charge transfer is typically lower than that of electrochemical systems composed of purely inorganic catalysts[23, 24].

Previous work has proposed that the bioinorganic interface is a key determinant of the CO_2-reducing rate[18]. Nevertheless, the dependence of the bioinorganic interface on electrochemical operational parameters including applied overpotential (η), biocatalyst loading and electrolyte pH is poorly understood. Here, we boosted the CO_2-reducing rate of our model Si nanowire/*S. ovata* platform by establishing a robust bacteria-nanowire interface (Fig. 1). We firstly found that the CO_2-reducing rate at high η was limited by poor bacteria-nanowire interface resulting from an inhospitable alkaline local environment. Tuning the bulk electrolyte pH mitigated the increase in local pH which strengthened the bioinorganic interface. Additionally, this supported higher biocatalyst loading on the nanowire electrode, forming a close-packed nanowire-bacteria cathode. The resulting close-packed biohybrid operated with CO_2-reducing current density ($J_{acetate}$) of 0.65 ± 0.11 mA cm^{-2} at ~-1.2 V *vs.* standard hydrogen electrode (SHE), with a faradaic efficiency of acetate ($FE_{aceatate}$) of ~80%. When coupled with a photovoltaic device, our system enabled solar-powered CO_2 fixation with solar-to-acetate efficiency of ~3.6% and an average daily acetate production rate of 44.3 g m^{-2} or 0.3 g L^{-1} over one week.

Results and discussions

Liu *et al.* previously demonstrated that Si nanowire arrays with a large surface area could be used to accommodate electrotrophic *S. ovata*[13]. Reducing equivalents generated from the light-harvesting electrodes powered *S. ovata* acetogenesis and thus enabled the conversion of CO_2 into extracellular acetate. In order to focus our scope on the bioinorganic interface and separate it from limitations of the semiconductor-based light harvesting process, we used highly doped conductive p^+ Si nanowire arrays as the cathode material and Pt wire as the counter electrode in

lieu of a TiO_2 photoanode. Initially, established inorganic phosphate buffered media[12, 18] was used as the electrolyte (initial pH 7.2), and an *S. ovata* suspension (4% v/v at OD_{545} of 0.38, Fig. S1) was inoculated into the cathodic chamber of the electrochemical cell (see Experimental procedures). With this set-up, we investigated the influence of the applied η on acetate production. At the onset of the electrochemical operation, we observed that *S. ovata* was sparsely distributed within the nanowire arrays (Fig. 2a) as each wire holds an average of ~2.6 cells (Fig. S2). This system was then subjected to sequentially elevated η from -0.71 V to -1.21 V *vs.* SHE. At low η from -0.71 V to -0.81 V *vs.* SHE, $FE_{aceatate}$ was close to 100% (Fig. 2b), indicating that the loaded bacteria could efficiently utilize a small flux of reducing equivalents to produce acetate. For example, at -0.81 V *vs.* SHE, the system achieved $FE_{aceatate}$ of 91 ± 19%, and $J_{acetate}$ of ~0.1 mA cm^{-2} that corresponds to an acetate turnover rate (TOR) of ~1.2 × 10^6 acetate molecules per second per cell (s^{-1} $cell^{-1}$). Our calculation is consistent with previous reported TOR of (1.0 ± 0.3) × 10^6 acetate molecules s^{-1} $cell^{-1}$ [13]. However, simply applying a more negative η did not correspondingly increase the acetate production rate. As we further increased the potential and thus the total current, $FE_{aceatate}$ dramatically decreased and $J_{acetate}$ plateaued at ~0.3 mA cm^{-2} (Fig. 2b). Specifically, only a 20% $FE_{aceatate}$ could be achieved when the total current density (J_{total}) reached ~1.2 mA cm^{-2}. This suggests that a majority of electrons were lost to H_2 evolution (see Fig. 1) instead of being directly taken up by the *S. ovata*. In addition, despite a high J_{total}, the peak $J_{acetate}$ of ~0.3 mA cm^{-2} is only comparable with the previously reported value[13]. This CO_2-fixation rate limit motivated our efforts to investigate the cause of the mismatched electron flux at the bioinorganic interface. Through thorough scanning electron microscopy (SEM) imaging, we found that the bacteria-electrode interface was deteriorated after electrochemical operation at -1.21 V *vs.* SHE. We observed large precipitates on the electrode

surface (Fig. S4a and b) possibly stemming from the inorganic compounds in the electrolyte. Energy-dispersive X-ray spectroscopy (EDS) confirmed that the precipitates were mainly composed of calcium phosphate and magnesium phosphate (Fig. S4c). This is triggered by high pH near the cathode surface due to accelerated proton consumption and inadequate mass transport at high current densities. Increases in local pH have been reported in bioelectrosynthesis as a driving factor for low production rates[27-29]. Methods to inspect pH microenvironments such as colorimetric dyes[30] have been investigated. However, as our nanostructured electrode complicates common pH measurements, we employed numerical 2-D simulations which reveal that the pH around nanowires increases to ~9.3 (Fig. S5). The alkaline environment not only brought about the formation of bulky precipitates but also created an incompatible environment for the biocatalysts[29, 31]. Altogether, this prevented the attachment of *S. ovata* to the electrode (Fig. S4), and thus impeded direct extracellular electron transfer (Fig. 1) lowering the overall CO_2-conversion rate[18]. In addition, the negatively charged electrode surface under alkaline condition[32, 33] could further deter adhesion of gram-negative *S. ovata*[34, 35]. Based on these findings, we increased the buffer capacity (5X phosphate concentration, initial pH 7.2, denoted as phosphate enhanced media) to mitigate the pH increase around the nanowire cathode[13]. However, enhancing the buffer capacity insignificantly improved the system's performance compared to that of the original electrolyte (Fig. S6a). At this point we observed that the *S. ovata* persistently escaped from the nanowire array and formed a biofilm on top after operation at -1.21 V *vs.* SHE (Fig. S6b and c). This observation implies that the local pH environment at high bias is still biologically unfavorable. Furthermore, evolved H_2 may delaminate *S. ovata* from the nanowire electrode[36]. Conclusively, these factors contribute to an obstinately poor bacteria-nanowire interface unable to maintain direct charge uptake at high η.

The formation of a biofilm suggests that the total amount of bacteria increased over the duration of the electrochemical experiment with the phosphate enhanced electrolyte (Fig. S6b and c), in contradistinction to the sparsely populated initial electrode. Chadwick and Jiménez Otero *et al.* previously verified that the most metabolically active bacteria in current-producing biofilms are those directly interfacing the electrode[37]. This could explain that although a biofilm forms, only those cells closely contacting the nanowires are robustly undertaking acetogenesis. In addition, Zhang *et al.* proposed that a close microbe-electrode interaction can increase the microbial CO_2-reducing rate[18]. Therefore, it is imperative to devise of a strategy to allow the bacteria to inhabit the nanowire array to fully take advantage of the large electrode surface area. Based on our simulation results, we found that the electrolyte with initial pH of 7.2 leads to a slightly basic environment (pH >9, at ~−1.2 V *vs.* SHE) at the electrode interface. Whereas an electrolyte with initial pH of 6.4 could more effectively mitigate the local pH change at a potential of ~−1.2 V *vs.* SHE (Fig. 3a). Therefore, we hypothesized that a combination of increased buffering capacity and initial lower electrolyte pH could support a robust bacteria-nanowire interface.

We monitored the development of *S. ovata* within the nanowire arrays over time (Fig. S7) employing an enhanced electrolyte with initial pH of 6.4. In order to facilitate the formation of a fully-embedded nanowire-bacteria system and thus allow more bacteria to contribute to acetate production, we inoculated the cathodic chamber with a higher concentration of bacteria initially (20% v/v at OD_{545} of 0.38, Fig. S1). After inoculation, the system was set at −0.8 V *vs.* SHE and the current density was maintained at 0.1 to 0.2 mA cm^{-2}, in order to provide a mild electrochemical environment that the bacteria can become accustomed to. Consequently, a close-packed nanowire-bacteria electrode was formed after a 3-day ramp-up stage with a bacteria density of ~13 cells per nanowire (Fig. S8).

Acetate production from CO_2 on this fully-embedded nanowire-bacteria system was evaluated at a series of sequentially increasing η. Phosphate enhanced electrolytes with three different initial pH values (6.4, 6.7 and 7.2) were used to systematically ascertain the influence of local pH at the electrode interface. The optimized hybrid system with different electrolyte pH all exhibited significantly enhanced $J_{acetate}$ (Fig. 3b) and $FE_{aceatate}$ (Fig. 3c) at high η compared to the initial results (Fig. 2b). The improvement was due to increased electron uptake by the densely packed biocatalysts around the nanowire electrodes. For all three electrolytes, $FE_{aceatate}$ is maintained around 60%~80% at potentials from −1.0 to −1.2 V *vs.* SHE. These results are considerably higher than those of the unoptimized system (Fig. 2b, 20~50%) where initially *S. ovata* was only sparsely distributed around the electrodes. Correspondingly, the peak $J_{acetate}$ was also increased from ~0.3 mA cm^{-2} to >0.45 mA cm^{-2}. For potentials ranging from -0.7 V to -1.1 V *vs.* SHE, the enhanced electrolyte with an initial pH of 6.7 supports the consistently greatest rate of CO_2-to-acetate conversion while the performance of the electrolytes with initial pH of 6.4 and 7.2 is similar. These results suggest that the electrolyte with initial pH 6.7 can sustain an optimal local microenvironment (including pH and preservation of Ni catalyst (Fig. S10)) for *S. ovata* during operating conditions up to -1.1 V *vs.* SHE. Furthermore, the electrolyte with initial pH of 6.4 has a more compelling effect at ~−1.2 V *vs.* SHE allowing for the greatest $J_{acetate}$. SEM inspection after electrochemical operation at ~-1.2 V *vs.* SHE revealed that the bacteria resided on top of electrodes, partially inside the nanowire arrays and densely embedded within the nanowire arrays for electrolytes with initial pH values of 7.2, 6.7 and 6.4, respectively (Fig. 3d to 3f). The different bacteria-nanowire associations are consistent with our simulation results (Fig. 3a), and indicate that the microbes migrate to their favorable environment under different electrochemical conditions. Correspondingly, the peak $J_{acetate}$ at ~-1.2 V *vs.* SHE was

boosted from 0.45 ± 0.05 mA cm^{-2} to 0.57 ± 0.02 mA cm^{-2} and finally up to 0.65 ± 0.11 mA cm^{-2} for electrolytes with initial pH values of 7.2, 6.7 and 6.4, respectively (Fig. 3b). The improved peak $J_{acetate}$ for initial pH 6.4 suggests that the close-packed bacteria-nanowire interface enhanced electron uptake, as evidenced by the $FE_{aceatate}$ at ~-1.2 V *vs.* SHE (Fig 3c). pH lower than 6.2 may dissolve the nickel coating on the electrode and therefore the electrolyte pH was not further lowered (Fig. S10).

The well-preserved bacteria-nanowire interface (Fig. 3f) allowed us to precisely estimate the bacteria density and thus calculate the TOR per bacterium at high η. At a CO_2-reducing rate of 0.65 ± 0.11 mA cm^{-2} with potential of −1.19 V *vs.* SHE, the TOR of *S. ovata* was (1.7 ± 0.5) × 10^6 acetate molecules s^{-1} $cell^{-1}$. For potentials higher than -1.2 V *vs.* SHE, we observed more hydrogen formation leading to a much reduced $FE_{aceatate}$ (Fig. S11). Altogether these results indicate that a potential of ~−1.2 V *vs.* SHE yielded a maximum CO_2-reducing current density of 0.65 ± 0.11 mA cm^{-2} under an optimized system with enhanced bacteria loading and a more bio-compatible local pH.

Following the optimization of our microbial electrochemical system we investigated whether our improvements would allow for efficient and sustained solar-to-chemical production[7-11, 13, 38, 39]. We coupled our close-packed nanowire-bacteria system with a photovoltaic device, as shown in the schematic diagram (Fig. 4a), and assessed long-term solar-driven CO_2-to-acetate production. The two-electrode electrochemical measurement with the close-packed hybrid system showed an onset voltage of ~1.8 V, and a ~3.2 V operating voltage was needed to reach a current density of ~1 mA cm^{-2} (Fig. 4b). Therefore, we employed a low-cost multi-junction Si solar cell (V_{oc} 4.7 V, I_{sc} 4.4 mA under one sun illumination) to provide enough voltage to drive the overall reaction. The expected operating current density of the integrated platform was determined by the

intersection of the *J-V* curves of both the solar cell (25 mW cm^{-2}, AM 1.5G illumination) and the hybrid system in a two-electrode configuration (Fig. 4b). The resulting value of ~0.82 mA cm^{-2} matches the optimal total current density found in the electrochemical experiments (Fig. S12).

The system was found to steadily produce acetate over one week, with daily solar-to-acetate efficiencies between 3~4% and an average acetate production rate of 44.3 g m^{-2} day^{-1} or 0.3 g L^{-1} day^{-1} (Fig. 4c). Control ^{13}C experiments confirmed the carbon source (Fig. S13) and a dark control experiment showed negligible acetate production (Fig. S14). The average 3.6% solar-to-acetate efficiency over seven days corresponds to an average CO_2-reducing current of 0.65 mA cm^{-2}, which is consistent with electrochemical measurements (Fig. 3b and Fig. S15). Overall, our results demonstrate a general route to improve the efficiency of bioelectrochemical CO_2 fixation by optimizing the bioinorganic interface. We namely show that a close bioinorganic interface plays a critical role in direct electron uptake in our model system. The insights obtained from this work can be combined with complementary approaches such as bacteria adaptation[19, 20], to further improve the CO_2 conversion rate and solar-to-chemical efficiency.

Experimental procedures

Preparation of p^+ Si nanowire array electrode

p^+ Si nanowire arrays were fabricated using reactive-ion etching of patterned single-crystalline Si wafers[13]. The 6-inch p^+-Si (boron) wafers (ρ ~0.001-0.005 Ω. cm) were obtained from Addison Engineering, Inc. After thoroughly cleaning in piranha and buffered hydrofluoric acid (BHF), the wafers were patterned with a photoresist dot array using a standard photolithography stepper. Then the wafers underwent inductive-coupled plasma deep reactive-ion etching (Surface Technology Systems. Inc) to yield uniform nanowire arrays (~20 μm long and ~900 nm in diameter). The Si nanowire arrays were thermally oxidized at 1,000 ºC for 3 hours, followed by etching in BHF for at least 5 minutes. The resulting thinned-down Si nanowires (700-800 nm in diameter) were subsequently coated with 5 nm of TiO_2 protective layer by atomic layer deposition (Picosun ALD), in order to maintain stable performance in a near neutral pH electrolyte for a long period of time. To facilitate the electron transfer from the cathode to the bacterium *S. ovata*[18], ~10 nm nickel (Ni) were sputtered at the surface of the resulting Si nanowire arrays (Edwards Inc.). For the electrode fabrication, ohmic contact to the device chip was made by rubbing Ga-In eutectic on its back side. Then the chip was fixed on Ti foil with conductive silver paint and carbon tape, resulting in good electrical connections. After that, the Si nanowire array samples were sealed using the nail polish, and the electrodes were ready for electrochemical characterizations.

Electrochemical characterization

S. ovata (DSM 2662) was originally obtained from the American Type Culture Collection (ATCC). An inoculum of *S. ovata* was grown in DSMZ 311 medium (betaine, casitone and resazurin omitted; yeast extract added) under strict anaerobic conditions with hydrogen as the electron donor (80% H_2 and 20% CO_2), as previous work described[12, 13, 18]. After 6 days of growth, the OD_{545} would reach 0.372 ± 0.012 (Fig. S1), and such hydrogen-grown bacteria were ready for the subsequent electrochemical CO_2 fixation. All electrochemical measurements were carried out using a home-built electrochemical setup. The setup is a two-chamber cell, with the working electrode and reference electrode (Ag/AgCl, 1M KCl, CH Instruments, Inc) in one chamber and a Pt wire as counter electrode in the other chamber. The two chambers were separated by a proton-exchange membrane (Nafion 212, FuelCellStore) when standard medium[12, 18] was used as the electrolyte. The nafion membrane was replaced by an anion-exchange membrane (AMI-7001S, kindly provided by Membranes International) when phosphate enhanced medium[13] was

used as the electrolyte, to facilitate the mass transport of the negatively-charged phosphate buffer ions and bicarbonate ions. The electrochemical characterization was performed using Gamry Interface 1000 potentiostats. Because of the change of the local pH over the entire experiment, $FE_{acetate}$ and $J_{acetate}$ were both characterized *vs.* SHE defined as following:

$$\text{V } \textit{vs.}\text{ SHE (V)} = \text{V } \textit{vs.}\text{ Ag/AgCl (V)} + 0.209\text{ (V)}$$

The overpotential η for CO_2 reduction is defined as the voltage difference between the applied electrochemical potential and the standard potential for CO_2 reduction into acetic acid:

$$\eta\text{ (V)} = \text{V } \textit{vs.}\text{ RHE (V)} - 0.143\text{ (V)}$$

Here RHE is the reversible hydrogen electrode potential defined as:

$$\text{V } \textit{vs.}\text{ RHE (V)} = \text{V } \textit{vs.}\text{ SHE (V)} + 0.059 \times \text{pH}$$

The nanowire-bacteria hybrids were realized in the cathode chamber using an organic-free minimal medium. Standard medium and phosphate-enhanced medium were both used as the electrolytes, to obtain different levels of proton mass transport, as mentioned above. For the phosphate-enhanced electrolyte, the initial pH value of the electrolyte was systematically tuned from 7.2 to 6.7 and finally 6.4, by adding certain amount of hydrochloric acid. The electrolyte was introduced to the electrochemical cell until its pH value was completely stabilized. We first ran abiotic chronoamperometry (-0.8 V *vs.* SHE) for 24 hours before bacteria inoculation, in order to allow the inert gas bubbling to remove O_2 residue in the cathode chamber. The hydrogen-grown *S. ovata* cells were then inoculated into the cathode chamber (4% v/v at OD_{545} of 0.38 for unoptimized system, and 20% v/v at OD_{545} of 0.38 for optimized system). The inoculation v/v ratio was adjusted accordingly if the OD_{545} slightly differed from 0.38. After bacteria inoculation, the electrochemical bias was kept at -0.8 V *vs.* SHE, and the dispersion was cultured under 80%N_2/10%H_2/10%CO_2 gas environment for 24 hours. At this stage, the electrolyte in the cathode chamber was turbid due to suspended bacteria. The bubbling gas was then switched to 80%N_2/20%CO_2. At this stage the electrochemical bias (-0.8 V *vs.* SHE) was maintained, and the Si nanowire electrode served as the sole electron source for the bacteria metabolism. The current density was maintained at ~0.15 mA cm^{-2} in order to provide a mild electrochemical environment for the bacteria to become accustomed to. After 24-hour incubation under 80%N_2/20%CO_2, 1/2 of the electrolyte in the cathode chamber was carefully replaced with fresh medium. After one more cycle of such medium exchange, the electrolyte in the cathode chamber became clear as most bacteria settled within the nanowire arrays and stable bacteria-nanowire interface was achieved. Next the hybrids were ready for electrochemical acetate production as follows.

Analysis of acetate production

Starting from less negative η, chronoamperometry was run for at least 12 hours at each electrochemical bias. After one chronoamperometry cycle was complete, an aliquot of the medium was sampled and a same amount of fresh medium was injected into the electrochemical cell. When nafion membrane was used, aliquots were only sampled from the cathode chamber for acetate analysis. On the other hand, aliquots were sampled from both the cathode chamber and anode chamber for acetate analysis when anion exchange membrane was used. Acetate concentration of the sample was quantified by proton nuclear magnetic resonance (^{1}H-qNMR) spectroscopy with sodium 3-

(trimethylsilyl)-2,2',3,3'-tetradeuteropropionate (TMSP-d4) as the internal standard. For the isotope labeling experiment, ^{13}C-labeled bicarbonate was used, and the same protocol was applied (Fig. S13). After obtaining the acetate concentration of each sample, $FE_{acetate}$ is calculated based on following equation:

$$FE_{acetate} = \frac{96485 \times 8 \times \text{incremental mole of acetic acid}}{\int \mathrm{I}\,\mathrm{dt}}$$

And the specific CO_2-reducing current density $J_{acetate}$ is defined as:

$$J_{acetate} = FE_{acetate} \times J_{total}$$

where J_{total} is the stabilized total current density during chronoamperometry (Fig. S3). In addition to acetate production, the electrons can be also used to produce biomass and H_2. As a result, $FE_{acetate} + FE_{biomass} + FE_{H_2} = 1$

Scanning electron microscopy (SEM) characterization

After the electrochemical characterizations were complete, the nanowire-bacteria hybrids were subjected to SEM characterization. First, an overnight bacteria fixation was performed by adding 2.5% glutaraldehyde directly to the medium in the cathode chamber[40]. Then the electrodes were washed with DI water followed by dehydration in increasing concentrations of ethanol (12.5%, 25%, 37.5%, 50%, 62.5%, 75%, 87.5%, 100%, 15 minutes each). Critical point drying (Tousimis, Inc.) was used to dry the nanowire-bacteria samples, in order to minimize the effect of the capillary force. Prior to imaging, the electrodes were cleaved along the middle and then sputtered with ~5 nm of Au (Denton Vacuum, LLC). The nanowire-bacteria hybrids were imaged at 5 keV/12 μA by field emission SEM (JEOL FSM6430). The density of *S. ovata* could be precisely estimated for the SEM image that showed clear bio-inorganic interface. For the sparsely polulated hybrids (Fig. 2a), the cell density was calculated by counting the number of cells within given areas of SEM images (Fig. S2). For the close-packed hybrids, the cell density was estimated by multiplying the density along the z-axis by the density over the x-y plane, as shown in Fig. S8.

Numerical simulation

The local pH within the nanowire arrays was simulated using the Electrochemical Module (steady state) of the COMSOL Multiphysics finite-element-analysis software package. In the 2-dimentional simulations, the nanowire's geometry (20 μm long, 0.8 μm in diameter and 2 μm pitch) is consistent with the experiment. To simplify the model geometry, we use five nanowires to represent the whole nanowire arrays (Figure 3a). Both phosphate buffer (H_3PO_4, $H_2PO_4^-$, HPO_4^{2-} and $PO4^{3-}$) and bicarbonate buffer (H_2CO_3, HCO_3^- and CO_3^{2-}) were accounted in the simulation. In the simulation, the mass transport is governed by the diffusion of ion species. At the nanowire's surface, the proton consumption rate is governed by Tafel equation[41] as following:

$$i = i_0 e^{\frac{-\alpha F \eta}{RT}}$$

where i_0 (exchange current density) and α (transfer coefficient) were both extracted from the experimental Tafel plot. Transfer of one electron corresponds to consumption of one proton. As high-concentration supporting ions were present in the actual electrolyte, the ion migration was not considered in this simulation. The stirring-induced

convection was simplified into a diffusion layer model, and the diffusion layer thickness (δ) was assumed to be 50 μm for all the involved ions[42, 43]. Beyond the diffusion layer, the concentrations of all the ions were constant determined by the boundary conditions. The boundary pH value was determined by the experimentally measured bulk pH value in the cathode chamber. Within the diffusion layer, the ion mass transport was governed by the Fick's law. The diffusion coefficients of all ion species were obtained from literature[41]. The equilibrium equations of the buffer systems applied to all the domains. All equilibrium constants were obtained from literature[41]. The minimum domain mesh size in the simulation is set to be 0.05 μm.

Solar-driven acetate production

For the solar-driven acetate production, a two-electrode configuration was used[44], where the nanowire-bacteria hybrids worked as the cathode and a Pt wire acted as the anode, respectively. Phosphate-enhanced medium (organic free, initial pH of 6.4) was used as the electrolyte. With the applied electrochemical bias maintained at -3.2 V, the hydrogen-grown *S. ovata* cells (20% v/v inoculum at OD_{545} of 0.38) were introduced into the cathode chamber, where the dispersion was first purged with 80%H_2/10%H_2/20%CO_2 gas mixture for 24 hours. The gas environment was then switched to 80%N_2/20%CO_2, and 1/2 of the electrolyte was replaced with fresh medium every 24 hours (repeated twice), similar to the electrochemical measurements mentioned above. After such medium exchange process, the established nanowire-bacteria hybrids were ready for the solar-driven acetate production. A commercial single-crystalline Si solar cell (KXOB22-01X8F) was obtained from Digi-key Corporation. A 300W Xenon arc lamp (Newport Corporation) with an AM1.5G filter was used for illumination. And the light intensity (25 mW cm^{-2}) was calibrated using a Si photodiode referenced to a NREL calibrated Si photodiode. Once the solar cell was connected to the electrodes, an aliquot of the medium was sampled every 24 hours for acetate quantification, and a same amount of fresh medium was injected into the electrochemical cell. The solar acetate production lasted for 7 days. The daily solar-to-acetate efficiency (ξ) was calculated based on the following equation:

$$\xi = \frac{8 \times 1.09(V) \times N_{acetate}(mol) \times 96485(C\ mol^{-1})}{I(mW\ cm^{-2}) \times A_{sc}(cm^2) \times 24 \times 3600(s)} \times 100\%$$

where 8 represents the number of electrons needed to produce one acetate molecule, 1.09 V is the thermodynamic potential needed to reduce CO_2 into acetate[13], $N_{acetate}$ is the amount of acetate produced in one day, I is the light intensity (25 mW cm^{-2}) and A_{sc} is the projected area of the Si solar cell (0.96 cm^2). Alternatively, ξ can also be expressed based on the calculated averaging $J_{acetate}$ as following:

$$\xi = \frac{1.09(V) \times Averaging\ J_{acetate}(mA\ cm^{-2}) \times A_{electrode}}{I(mW\ cm^{-2}) \times A_{sc}(cm^2)} \times 100\%$$

Where $A_{electrode}$ is the projected area of our Si nanowire electrode (1.2 cm^2).

Acknowledgements

This work was supported by the National Aeronautics and Space Administration (NASA), under grant numbered NNX17AJ31G. The authors would like to acknowledge Dr. Long Hu, Dr. Kelsey Sakimoto, Dr. Hao Liu, Dr. Yingbo Zhao, Dr. Yifan Li, Tom Tacken, Anthony Abel, Mathangi Soundararajan and Aaron Berliner for helpful discussions. The authors thank the Marvell Nanofabrication Laboratory for use of their facilities. Y. S. acknowledges the graduate fellowship support from USTC-Suzhou Industrial Park. S. C. B. thanks the Philomathia foundation.

Author contributions

Y. S. and P. Y. designed the experiments. Y. S., S. C. B. and Q. K. fabricated the silicon nanowire electrodes. Y. S., S. C. B., J. M. K., Y-x. S. and C. L. performed the bacteria culturing and incubation. Y. S., S. C. B., J. M. K., Y-x. S. and H. Z. did the electrochemical and solar-driven experiments. Y. S., D. L. and Y. C. did the numerical calculation. Y. S., S. C. B., Y-x. S. and P. Y. co-wrote the paper. All authors discussed the results and revised the manuscript.

Declaration of interests

The authors declare no competing financial interests.

References

1. Chiappini, C., Rosa, E. D., Martinez, J. O., Liu, X., Steele, J., Stevens, M. M., and Tasciotti, E. (2015). Biodegradable silicon nanoneedles delivering nucleic acids intracellularly induce localized in vivo neovascularization. Nature Mater. *14*, 532-539.
2. Sharei, A., Zoldan, J., Adamo, A., Sim, W. Y., Cho, N., Jackson, E., Mao, S., Schneider, S., Han, M., Lytton-Jean, A., et al. (2013). A vector-free microfluidic platform for intracellular delivery. Proc. Natl. Acad. Sci. U.S.A. *110*, 2082-2087.
3. Tian, B., Cohen-Karni, T., Qing, Q., Duan, X., Xie, P., and Lieber, C. M. (2010). Three-Dimensional, flexible nanoscale field-effect transistors as localized bioprobes. Science *329*, 830-834.
4. Xie, C., Lin, Z., Hanson, L., Cui, Y., and Cui, B. (2012). Intracellular recording of action potentials by nanopillar electroporation. Nature Nanotech. *7*, 185-190.
5. Logan, B. E. (2009). Exoelectrogenic bacteria that power microbial fuel cells. Nature Rev. Microbiol. *7*, 375–381.
6. Lovley, D. R. (2006). Bug juice: harvesting electricity with microorganisms. Nature Rev. Microbiol. *4*, 497-508.
7. Sakimoto, K. K., Wong, A. B., and Yang, P. (2016). Self-photosensitization of nonphotosynthetic bacteria for solar-to-chemical production. Science *351*, 74-77.
8. Zhang, H., Liu, H., Tian, Z., Lu, D., Yu, Y., Cestellos-Blanco, S., Sakimoto, K. K., and Yang, P. (2018). Bacteria photosensitized by intracellular gold nanoclusters for solar fuel production. Nature Nanotech. *13*, 900-905.
9. Nichols, E. M., Gallagher, J. J., Liu, C., Su, Y., Resasco, J., Yu, Y., Sun, Y., Yang, P., Chang, M. C. Y., and Chang, C. J. (2015). Hybrid bioinorganic approach to solar-to-chemical conversion. Proc. Natl. Acad. Sci. U.S.A. *112*, 11461-11466.
10. Liu, C., Colón, B. C., Ziesack, M., Silver, P. A., and Nocera, D. G. (2015). Water splitting–biosynthetic system with CO_2 reduction efficiencies exceeding photosynthesis. Science *352*, 1210-1213.
11. Zhang, T. (2015). More efficient together. Science *350*, 738-739.
12. Nevin, K. P., Woodard, T. L., Franks, A. E., Summers, Z. M., and Lovley, D. R. (2010). Microbial electrosynthesis: feeding microbes electricity to convert carbon dioxide and water to multicarbon extracellular organic compounds. mBio *1*, 1-4.
13. Liu, C., Gallagher, J. J., Sakimoto, K. K., Nichols, E. M., Chang, C. J., Chang, M. C. Y., and Yang, P. (2015). Nanowire-bacteria hybrids for unassisted solar carbon dioxide fixation to value-added chemicals. Nano lett. *15*, 3634-3639.
14. Rabaey, K., and Rozendal R. A. (2010). Microbial electrosynthesis-revisiting the electrocial route for microbial production. Nature Rev. Microbiol. *8*, 706-716.
15. Lewis, N. S., and Nocera, D. G. (2006). Powering the planet: chemical challenges in solar energy utilization. Proc. Natl. Acad. Sci. U.S.A. *103*, 15729-15735.
16. Marshall, C. W., Ross, D. E., Fichot, E. B., Norman, R. S., and May, H. D. (2013). Long-term operation of microbial electrosynthesis systems improves acetate production by autotrophic microbiomes. Environ. Sci. Technol. *47*, 6023-6029.

17. Cui, M., Nie, H., Zhang, T., Lovley, D. R., and Russell, T. P. (2017). Three-dimensional hierarchical metal oxide–carbon electrode materials for highly efficient microbial electrosynthesis. Sustainable Energy & Fuels *1*, 1171-1176.
18. Zhang, T., Nie, H., Bain, T. S., Lu, H., Cui, M., Snoeyenbos-West, O. L., Franks, A. E., Nevin, K. P., Russell, T. P., and Lovley, D. R. (2013). Improved cathode materials for microbial electrosynthesis. Energy & Environ. Sci. *6*, 217-224.
19. Ammam, F., Tremblay, P. L., Lizak, D. M., and Zhang, T. (2016). Effect of tungstate on acetate and ethanol production by the electrosynthetic bacterium *Sporomusa ovata*. Biotechnol. Biofuels *9*, 163.
20. Tremblay, P. L., Hoglund, D., Koza, A., Bonde, I., and Zhang, T. (2015). Adaptation of the autotrophic acetogen *Sporomusa ovata* to methanol accelerates the conversion of CO_2 to organic products. Sci. Rep. *5*, 16168.
21. Patil, S. A., Arends, J. B. A., Vanwonterghem, I., Meerbergen, J. V., Guo, K., Tyson, G. W., and Rabaey, K. (2015). Selective enrichment establishes a stable performing community for microbial electrosynthesis of acetate from CO_2. Environ. Sci. Technol. *49*, 8833-8843.
22. Su, Y., Liu, C., Brittman, S., Tang, J., Fu, A., Kornienko, N., Kong, Q., and Yang, P. (2016). Single-nanowire photoelectrochemistry. Nature Nanotech. *11*, 609-612.
23. Liu, M., Pang, Y., Zhang, B., De Luna, P., Voznyy, O., Xu, J., Zheng, X., Dinh, C. T., Fan, F., Cao, C., et al. (2016). Enhanced electrocatalytic CO_2 reduction via field-induced reagent concentration. Nature *537*, 382-386.
24. Ross, M. B., De Luna, P., Li, Y., Dinh, C. T., Kim, D., Yang, P., and Sargent, E. H. (2019). Designing materials for electrochemical carbon dioxide recycling. Nature Catal. *2*, 648-658.
25. Kumar, A., Hsu, L. H. H., Kavanagh, P., Barrière, F., Lens, P. N. L., Lapinsonnière, L., Lienhard V, J. H., Schröder, U., Jiang, X., and Leech, D. (2017). The ins and outs of microorganism-electrode electron transfer reactions. Nature Rev. Chem. *1*, 24.
26. Tremblay, P. L., Angenent, L. T., and Zhang, T. (2017). Extracellular electron uptake: among autotrophs and mediated by surfaces. Trends Biotechnol. *35*, 360-371.
27. LaBelle, E. V., and May, H. D. (2017). Energy efficiency and productivity enhancement of microbial electrosynthesis of acetate. Front. Microbiol. *8*, 756.
28. Jourdin, L., Freguia, S., Flexer, V., and Keller, J. (2016). Bringing high-rate, CO_2-based microbial electrosynthesis closer to practical implementation through improved electrode design and operating conditions. Environ. Sci. Technol. *50*, 1982-1989.
29. Mohanakrishna, G., Seelam, J. S., Vanbroekhoven, K., and Pant, D. (2015). An enriched electroactive homoacetogenic biocathode for the microbial electrosynthesis of acetate through carbon dioxide reudction. Faraday Discuss. *183*, 445-462.
30. Qu, F., Li, N. B., and Luo, H. Q. (2013). Highly sensitive fluorescent and colorimetric pH sensor based on polyethylenimine-capped silver nanoclusters. Langmuir. *29*, 1199-1205.
31. Möller, B., OƁmer, R., Howard, B. H., Gottsehalk, G., and Hippe, H. (1984). *Sporomusa*, a new genus of gram-negative anaerobic bacteria including *Sporomusa sphaeroides* spec. nov. and *Sporomusa ovata* spec. nov.* Arch. Microbiol. *139*, 388-396.
32. Holmberg, J. P., Ahlberg, E., Bergenholtz, J., Hassellov, M., and Abbas, Z. (2013). Surface charge and interfacial potential of titanium dioxide nanoparticles: experimental and theoretical investigations. J. Colloid Interface Sci. *407*, 168-176.
33. Preočanin, T., and Kallay, N. (2006). Point of zero charge and surface charge density of TiO_2 in aqueous electrolyte solution as obtained by potentiometric mass titration. Croatica Chemica Acta *79*, 95-106.
34. Sára, M., and Sleytr, U. B. (2000). S-layer proteins. J. Bacteriol. *182*, 859-868.
35. Beverridge, T. J. (1999). Structures of gram-negative cell walls and their derived membrane vesicles. J. Bacteriol *181*, 4725-4733.

36. Blanchet, E., Duquenne, F., Rafrafi, Y., Etcheverry, L., Erable, B., and Bergel, A. (2015). Importance of the hydrogen route in up-scaling electrosynthesis for microbial CO_2 reduction. Energy Environ. Sci. *8*, 3731-3744.
37. Chadwick, G. L., Otero, F. J., Gralnick, J. A., Bond, D. R., and Orphan, V. J. (2019). NanoSIMS imaging reveals metabolic stratification within current-producing biofilms. Proc. Natl. Acad. Sci. U.S.A. *116*, 20716-20724.
38. Zhang, J. Z., Bombelli, P., Sokol, K. P., Fantuzzi, A., Rutherford, A. W., Howe, C. J., and Reisner, E. (2018). Photoelectrochemistry of photosystem II *in Vitro* vs. *in Vivo*. J. Am. Chem. Soc. *140*, 6-9.
39. Kornienko, N., Zhang, J. Z., Sakimoto, K. K., Yang, P., and Reisner, E. (2018). Interfacing nature's catalytic machinery with synthetic materials for semi-artificial photosynthesis. Nature Nanotech. *13*, 890-899.
40. Sakimoto, K. K., Liu, C., Lim, J., and Yang, P. (2014). Salt-induced self-assembly of bacteria on nanowire arrays. Nano lett. *14*, 5471-5476.
41. Bard, A. J., and Faulkner, L. R. (2000). Electrochemical methods: fundamentals and applications, 2nd ed., (John Wiley&Sons, Inc. press).
42. Walker, R., and Holt, N. S. (1984). Determination of the Nernst diffusion layer thickness in the hydroson agitation tank. Surface Technology *22*, 165-174.
43. Tobias, C. W., Eisenberg, M., and Wilke, C. R. (1952). Diffusion and convection in electrolysis-a theoretical review. Electrochemistry of ionic crystals *99*, 359-365.
44. Luo, J., Im, J. H., Mayer, M. T., Schreier, M., Nazeeruddin, M. K., Park, N. G., Tilley, S. D., Fan, H. J., and Grätzel, M. (2014). Water photolysis at 12.3% efficiency via perovskite photovoltaics and earth-abundant catalysts. Science *345*, 1593-1596.

Figures

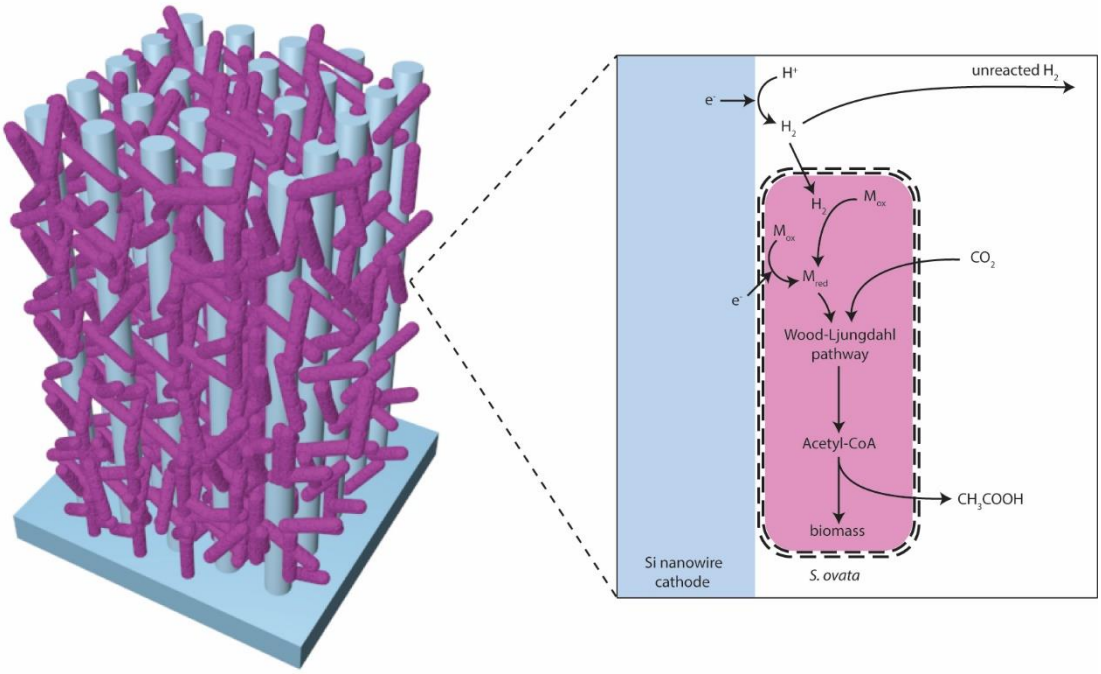

Figure 1. Schematics of the close-packed nanowire-bacteria hybrid system (left) and the reaction pathway (right). The electrons are transferred (via either direct pathway[14, 25, 26] or H_2-mediated pathway[7, 9, 10]) from the Si nanowire cathode to *S. ovata* to generate the intracellular reducing equivalents (M_{red}). The reducing equivalents are finally passed on to the Wood-Ljungdahl pathway to produce acetate and biomass.

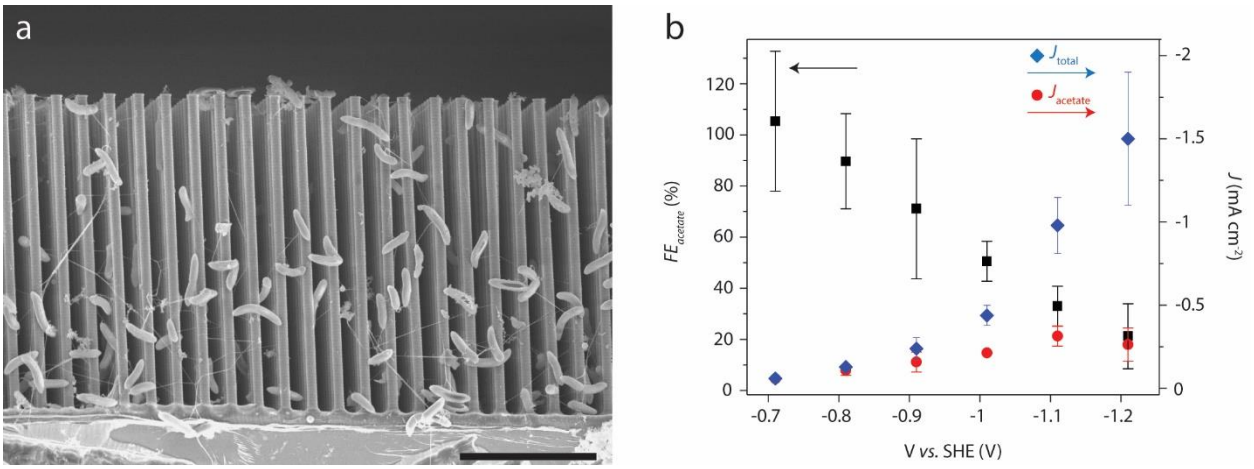

Figure 2. The imaging and electrochemical characterizations of nanowire-bacteria hybrids before optimization. a, SEM image of the nanowire-bacteria hybrids (fixed at -0.81 V *vs.* SHE) with standard electrolyte (initial pH value of 7.2) and 4% v/v bacteria inoculation. **b,** The electrochemical performance of the nanowire-bacteria hybrids at different η (starting from less negative η, n=3). $J_{acetate}$ is defined as J_{total} (Fig. S3) multiplied by $FE_{aceatate}$. The scale bar is 10 μm.

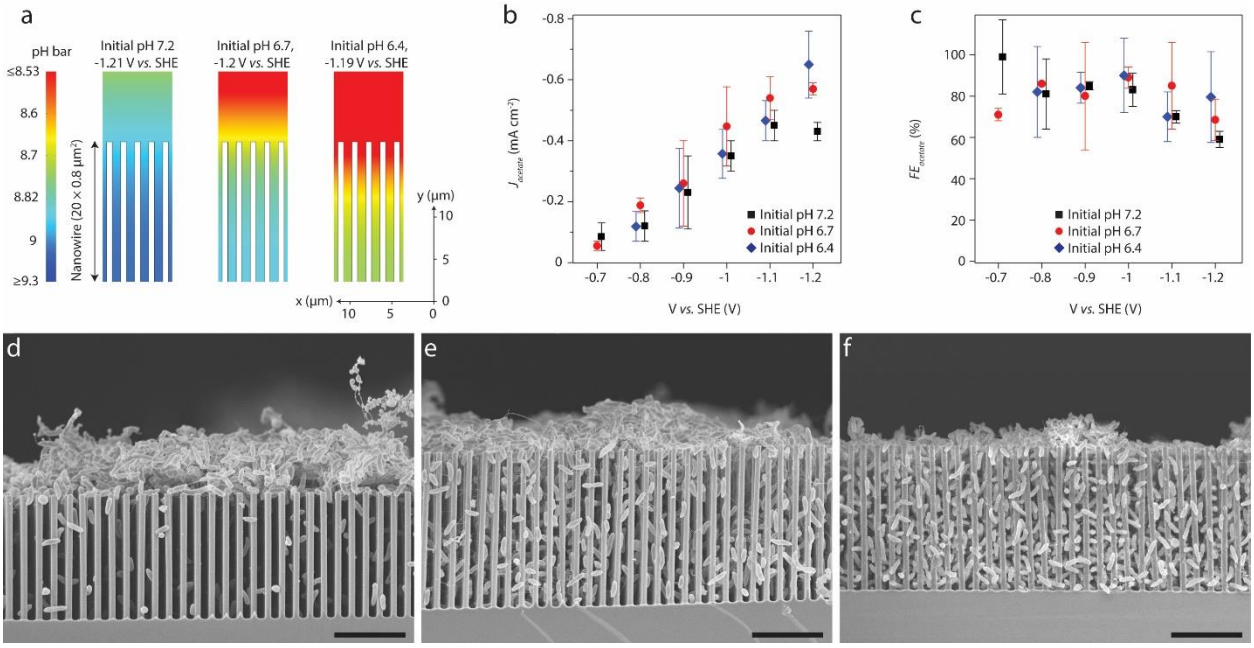

Figure 3. The electrochemical performance and SEM images of nanowire-bacteria hybrids with optimized bacteria loading and electrolyte composition. a, Numerical simulations demonstrate that the transition of initial pH values of phosphate enhanced electrolytes from 7.2, 6.7 to 6.4 gradually lowered the pH around the nanowires from >9 to <8.7. The boundary pH values in the simulations were determined by the experimentally measured bulk pH values in the cathode chamber (Fig S9). **b-c,** Bias-dependent $J_{acetate}$ (**b**) and $FE_{aceatate}$ (**c**) of the fully embedded nanowire-bacteria hybrids using phosphate enhanced electrolytes with different initial pH values (n=3 for each case). **d-f,** The SEM images of the fully embedded nanowire-bacteria hybrids after operation at ~-1.2 V vs. SHE using electrolytes with different initial pH values. A clear transition from a top aggregation of bacteria (initial pH value of 7.2, panel d) to a semi-close-packed structure (initial pH value of 6.7, panel e), and finally to a close-packed structure (initial pH value of 6.4, panel f) was observed. The scale bar is 10 μm.

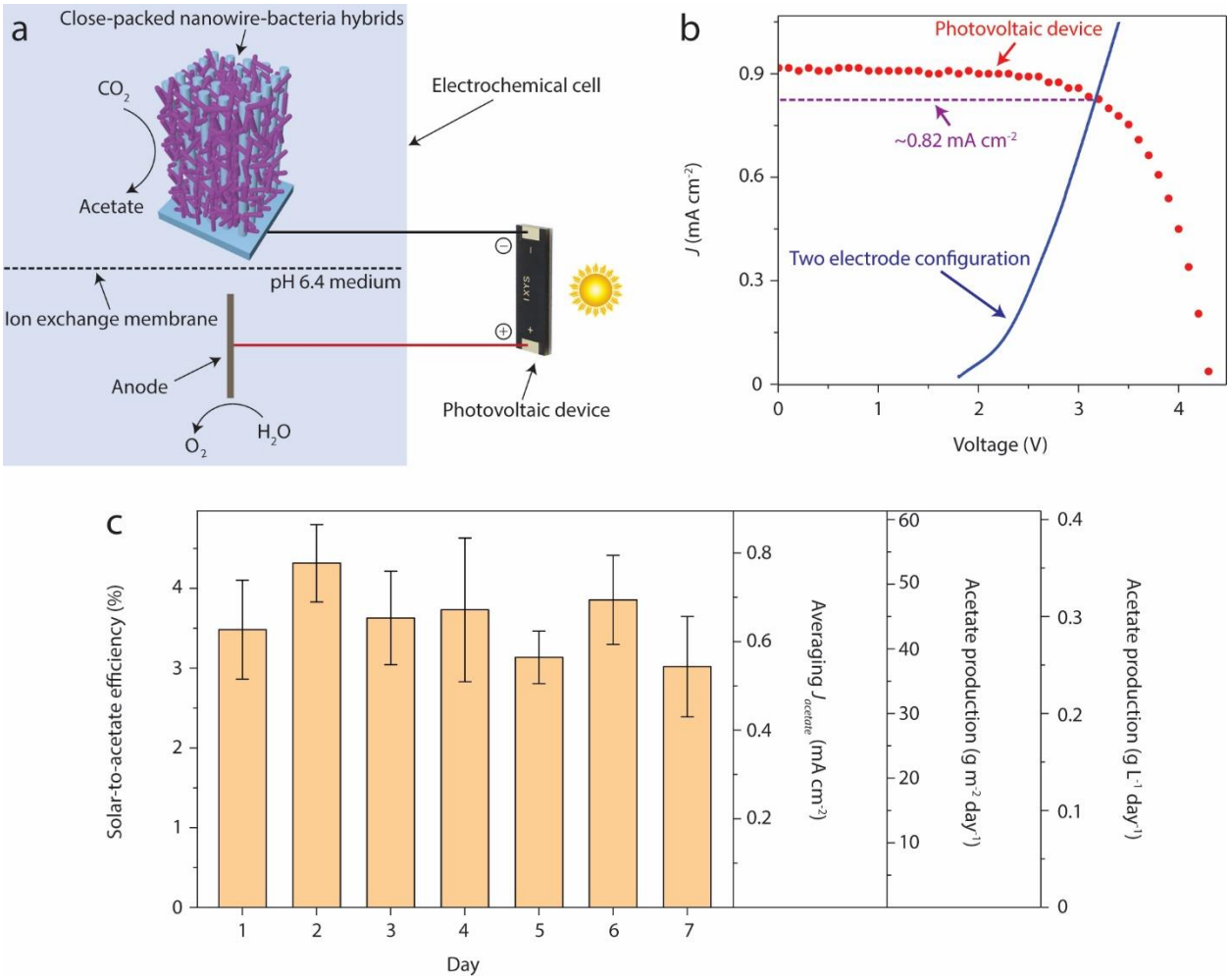

Figure 4. Integrating close-packed nanowire-bacteria hybrids with Si solar cell for solar-driven acetate production. a, Schematic illustration of the integrated device mimicking photosynthesis. **b,** *J-V* curves of a multi-junction Si solar cell under 25 mW/cm^2, AM1.5G illumination, and the close-packed nanowire-bacteria hybrids in a two-electrode configuration. **c,** The acetate production and solar efficiency of the device over one week (n=3). The four y axes represent (from left to right) the solar-to-acetate energy conversion efficiency, the calculated daily averaging $J_{acetate}$, the daily acetate production based on electrode projected area and the daily acetate production per unit volume, respectively.

Supplemental Figures:

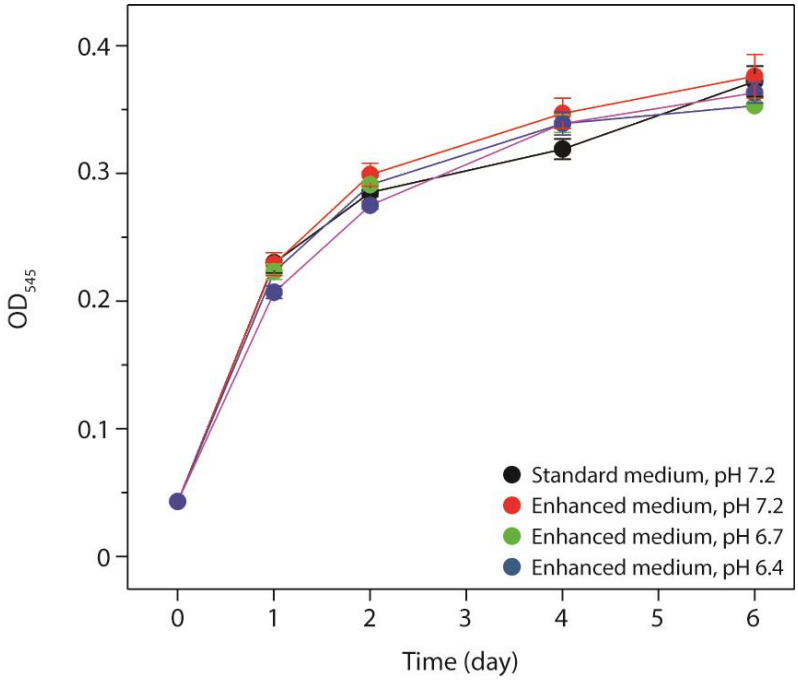

Figure S1. Growth curves of *S. ovata* using different growth mediums. Black curve displays *S. ovata* growth under strict anaerobic condition (80% H_2 and 20% CO_2) in standard growth medium (betaine, casitone and resazurin omitted; yeast extract added (see Experimental Procedures)). After 6 days of growth, the OD_{545} would reach 0.372±0.012. The v/v ratio of cathode inoculation (4% v/v for unoptimized system and 20% v/v for optimized system) was based on OD_{545} of 0.38. And the ratio would be adjusted accordingly if the OD_{545} differed from 0.38. The growth curves show similar trends when the pH value of phosphate enhanced growth medium is lowered (red, green and blue curves). $n \geq 3$.

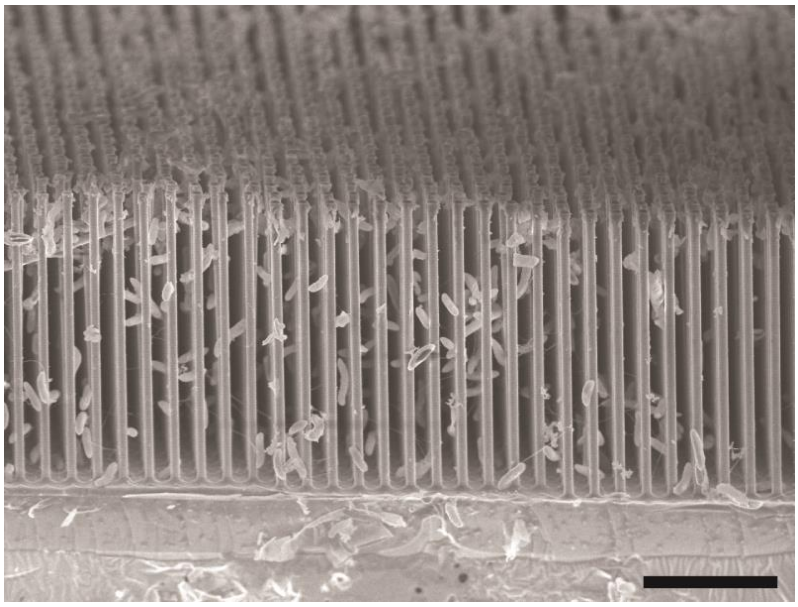

Figure S2. A representative tilting SEM image of the unoptimized nanowire-bacteria hybrid system (4% v/v bacteria inoculation, standard medium, initial pH 7.2) at -0.81 V *vs.* SHE. The cell density could be calculated by counting the number of cells within given areas of these SEM images, and the resulting density is 2.62±0.17 per nanowire or 0.655±0.04 μm^{-1} (n=3). The scale bar is 10 μm.

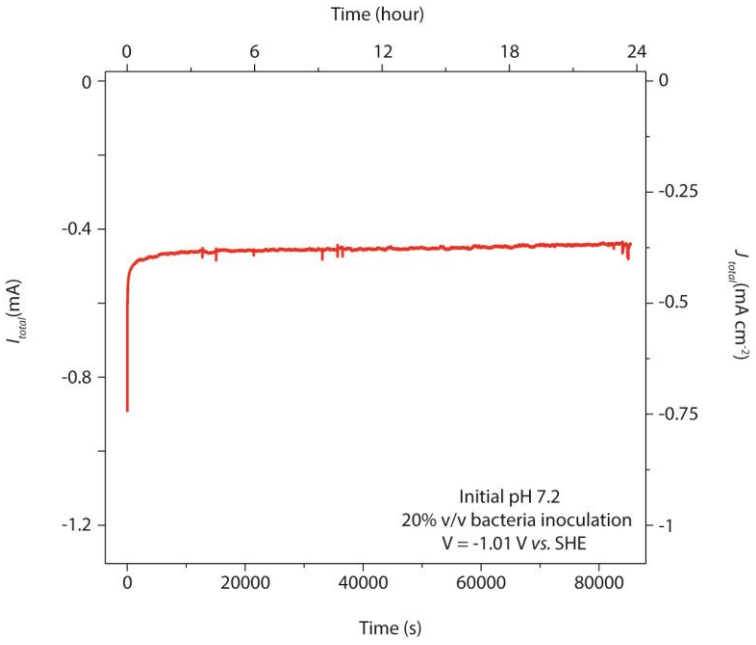

Figure S3. Chronoamperometry characterization. A representative chronoamperometry curve showed that I_{total} (so as J_{total}) would reach a stable value typically within 10000 seconds (~3 hours) after initialization. Here I_{total} (mA) and time (s) represent the original, non-processed unit in the raw data file.

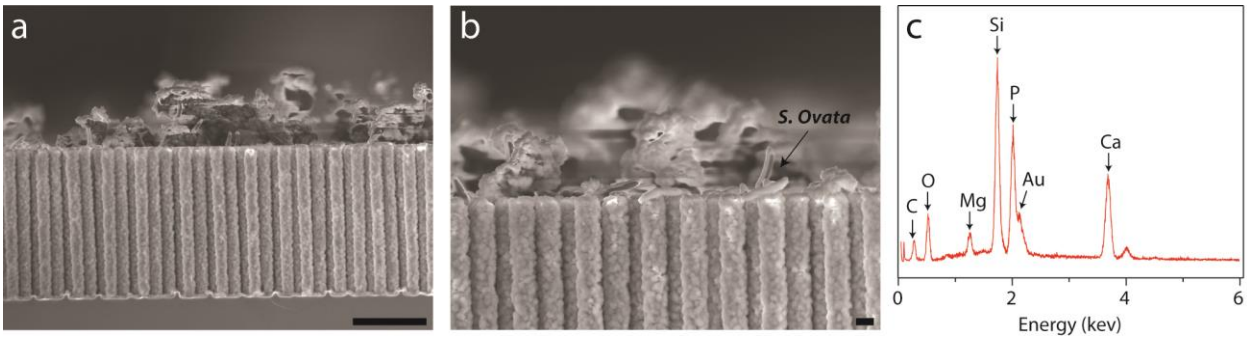

Figure S4. Characterization of the precipitate on the nanowire surface. (a) Low-magnification and (b) high-magnification SEM images showed the precipitate formed on the nanowire surface at potential of -1.21 V *vs.* SHE when standard medium (initial pH 7.2) was used as the electrolyte. *S. ovata* also escaped away from the nanowire arrays. (c) The EDS data suggests that the precipitate consisted mainly of $Ca_3(PO_4)_2$ and $Mg_3(PO_4)_2$, while $CaCO_3$, $MgCO_3$ and $Mg(OH)_2$ might also exist due to the increasing local pH as described in Fig. S5. The composition of the precipitate was not quantified since EDS is not accurate for low atomic number elements (C and O)[1, 2]. Given the K_{sp} values of all the potential precipitates[3] and the concentrations of Ca^{2+}, Mg^{2+}, phosphate buffer and bicarbonate in the electrolyte, the precipitating order is $Ca_3(PO_4)_2 > Mg_3(PO_4)_2 > CaCO_3 > MgCO_3 > Mg(OH)_2$.

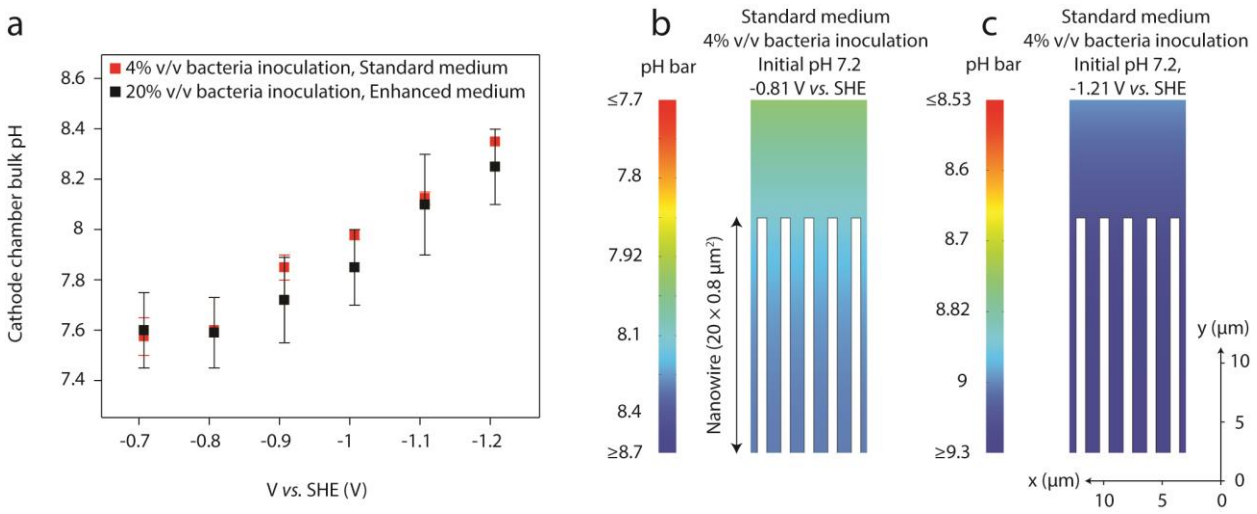

Figure S5. Additional numerical simulations of the local pH using Comsol multi-physics. The simulations were carried out under (b) standard medium, 4% v/v bacteria inoculation, -0.81 V *vs.* SHE and (c) standard medium, 4% v/v bacteria inoculation, -1.21 V *vs*. SHE respectively, where the boundary pH values were determined by the experimentally measure pH values in the cathode chamber (red rectangle in a). The use of phosphate enhanced medium yielded less alkaline bulk pH in the cathode chamber. (b) is consistent with the well-interfaced hybrids observed in Fig. 2a and Fig S2. And (c) is consistent with the observed precipitate in Fig. S4.

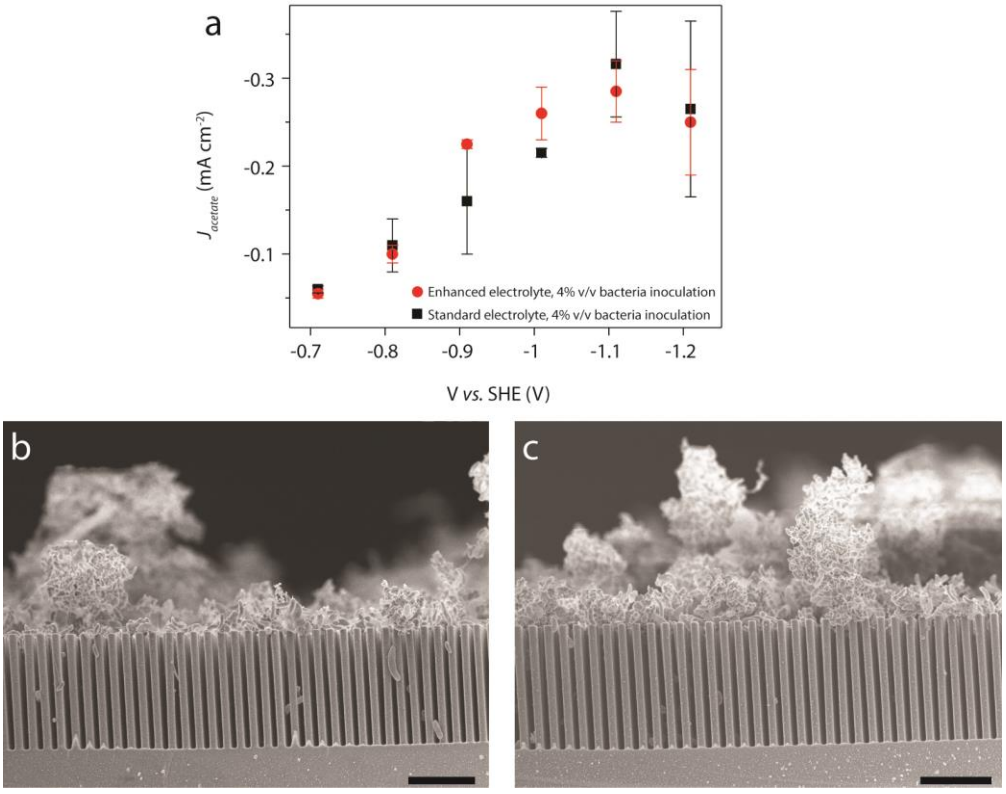

Figure S6. Performance and imaging of the nanowire-bacteria hybrids with 4% v/v bacteria inoculation and phosphate enhanced electrolyte. (a) $J_{acetate}$ showed insignificant improvement at high bias (from -1.01 V to -1.21 V *vs.* SHE) when standard electrolyte (initial pH 7.2, n=3) was simply replaced by phosphate enhanced electrolyte (initial pH 7.2, n=3). (b) and (c) Representative SEM images of the hybrids after operation at potential of -1.21 V *vs.* SHE showed that although no precipitate was observed, most of the bacteria stayed on the top of the nanowires, leading to a poor bio-inorganic interface. Statistical analysis of the biofilm thickness gave an estimate of ~4 μm, corresponding to an estimate of projected bacteria density of ~5 cells per nanowire.

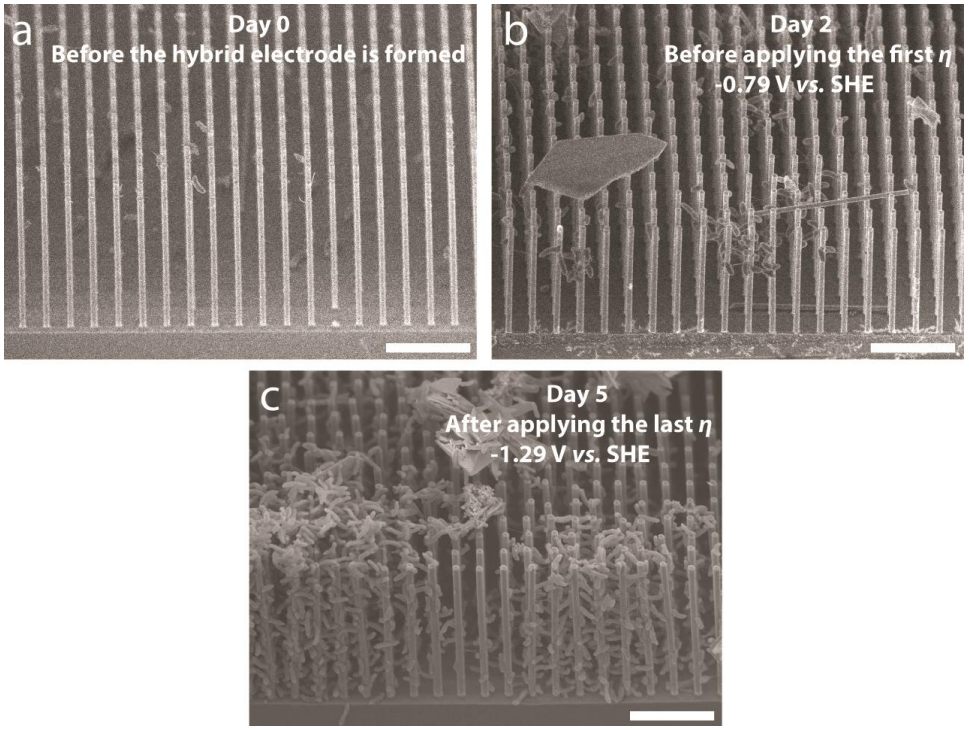

Figure S7. SEM images showed the development of *S. ovata* within the nanowire arrays over time when 4% v/v bacteria inoculation was used. At the first-two-day initialization stage, moderate current and electrochemical potential (-0.1~0.2 mA/cm^2 and ~−0.8 V *vs.* SHE) allowed the adaptation of bacteria and formation of the hybrid electrode. When an increasingly more negative η was applied starting from day 3, significant bacteria growth was observed. In order to obtain a well-interfaced hybrid system to monitor the bacteria development, phosphate enhanced media (initial pH of 6.4) was used as the electrolyte.

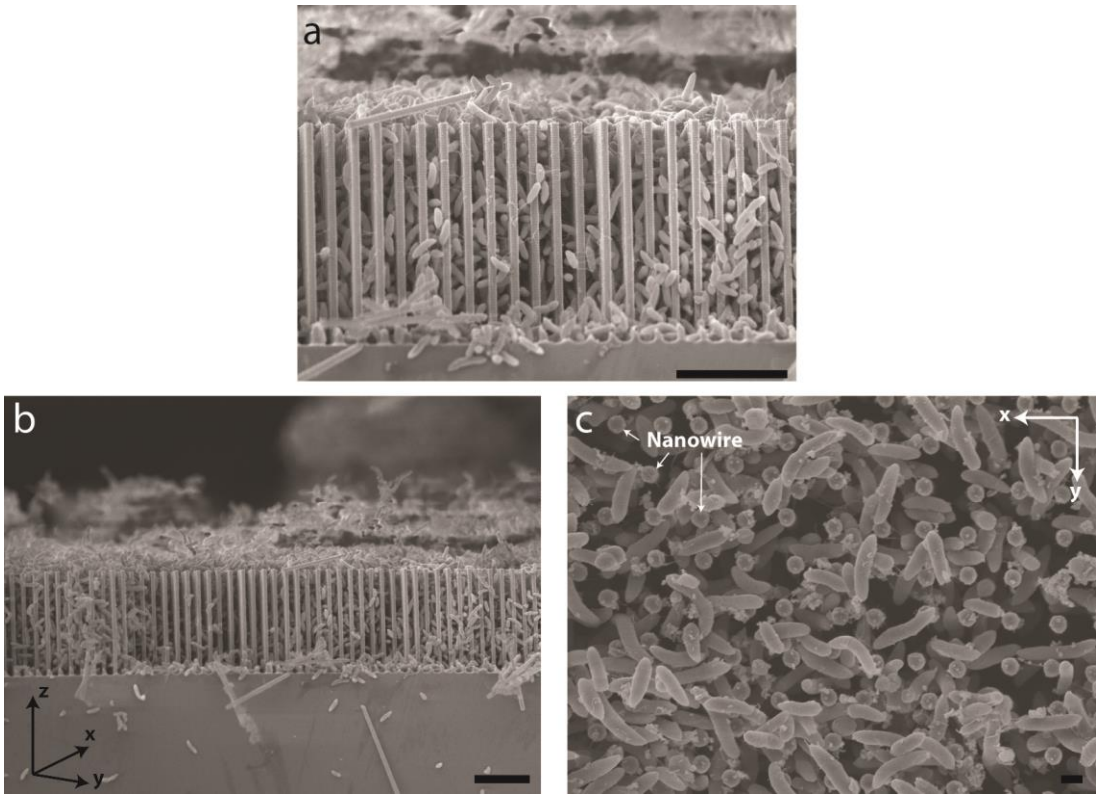

Figure S8. SEM images of the close-packed nanowire-bacteria hybrids. Representative high-magnification cross-sectional (a), low-magnification cross-sectional (b) and top-down view (c) SEM images clearly showed that the close-packed nanowire-bacteria biohybrid was obtained, after the system was inoculated with 20% v/v bacteria suspension and operated at ~-0.1-0.2 mA/cm^2 for 3 days. The cell density of the close-packed hybrids could be estimated by multiplying the bacteria density along the Z-axis (~10, estimated from cross-sectional images) by the bacteria density on the x-y plane (~1.3 per nanowire, from top-to-down images). The resulting bacteria loading density was about 13 per nanowire. The scale bars are 10 μm (panel a and b) and 1 μm (panel c), respectively.

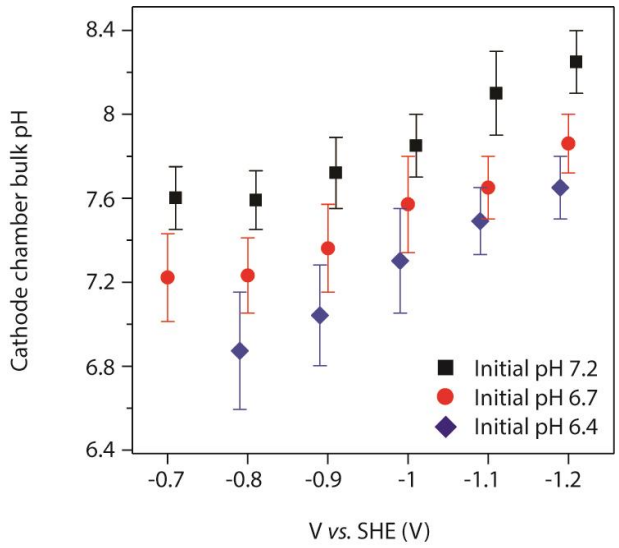

Figure S9. The bulk pH values in the cathode chamber as a function of the applied electrochemical potential. Phosphate enhanced media with different initial pH values were used as the electrolytes. The pH of each aliquot was analyzed with a carefully calibrated pH meter (Mettler Toledo Seveneasy 8603). The bulk pH values tended to increase as a more negative potential was applied, because of the limited mass transport of buffer species across the ion-exchange membrane. The difference in initial pH values could lead to a consistent bulk pH difference over the entire experiment, because the CO_2/N_2 bubbling rate was slow so that the extra CO_2 could not balance the initial pH difference.

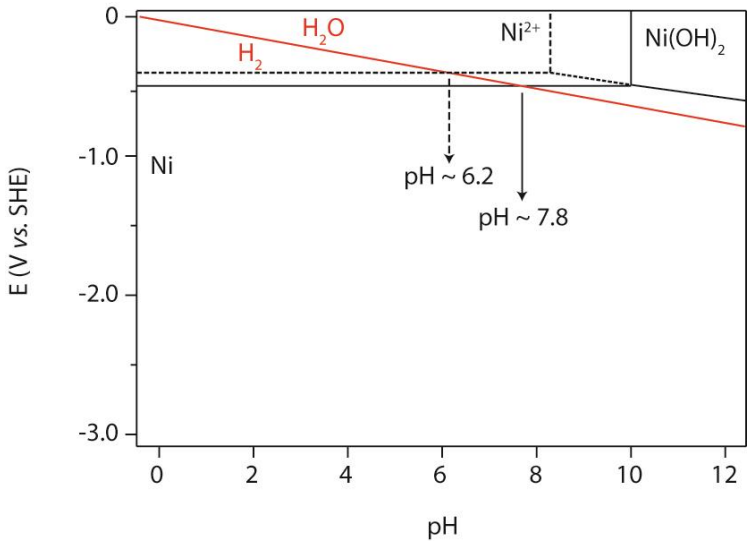

Figure S10. Pourbaix diagram of the Ni-water system. The pourbaix diagram was calculated based on the initial Ni^{2+} concentration (10^{-7} mol/L, calculated based on the DSMZ medium, solid line in the figure) and the dissolved Ni^{2+} concentration if all the sputtered Ni on the nanowires was assumed to be dissolved (~10^{-4} mol/L, dashed line in the figure). When the pH was higher than 7.8, all the sputtered Ni on the nanowires should be well preserved. If the pH value was lower than 7.8, a part of the sputtered Ni would be dissolved before electrochemical potential was applied, which hindered electron transfer in the following electrochemical measurement. The percentage of the dissolved Ni increased as pH decreased. For pH lower than 6.2, all the sputtered Ni on the nanowires would be dissolved before electrochemical potential was applied. The dissolved Ni might be re-deposited on the nanowire surface when the electrochemical potential was applied during choronoamperometry operation.

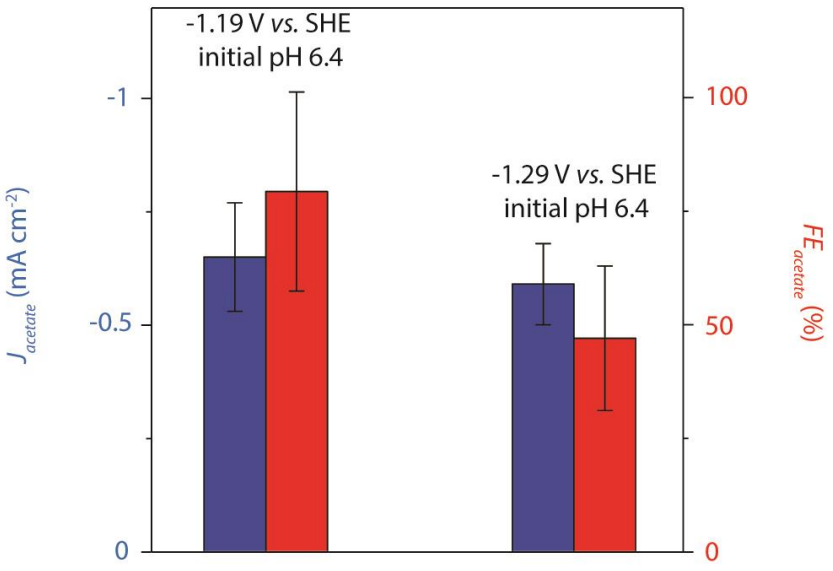

Figure S11. Comparison in $J_{acetate}$ and $FE_{acetate}$ for nanowire-bacteria hybrids (using phosphate enhanced electrolytes, initial pH 6.4) under electrochemical potentials of -1.19 V *vs.* SHE and -1.29 V *vs.* SHE

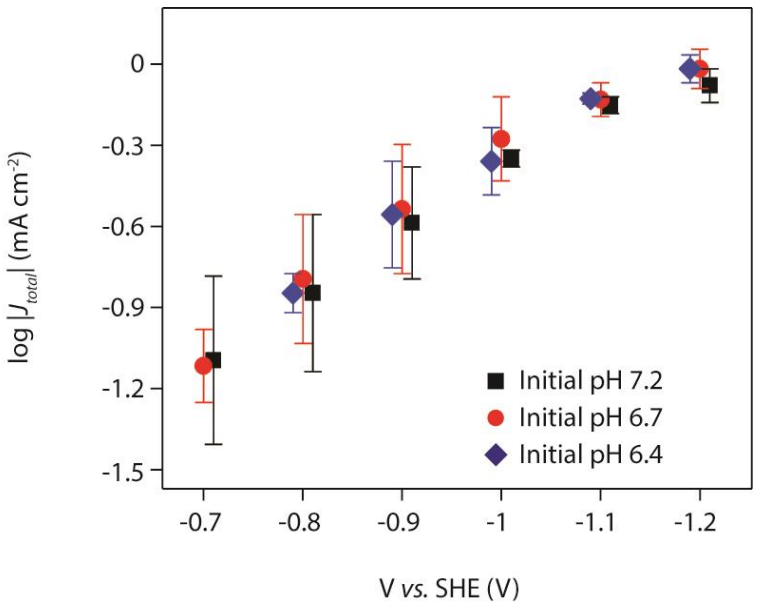

Figure S12. Comparison in J_{total} for nanowire-bacteria hybrids using phosphate enhanced electrolytes with different initial pH values. The bias-dependent J_{total} overall didn't change much with the different initial pH values.

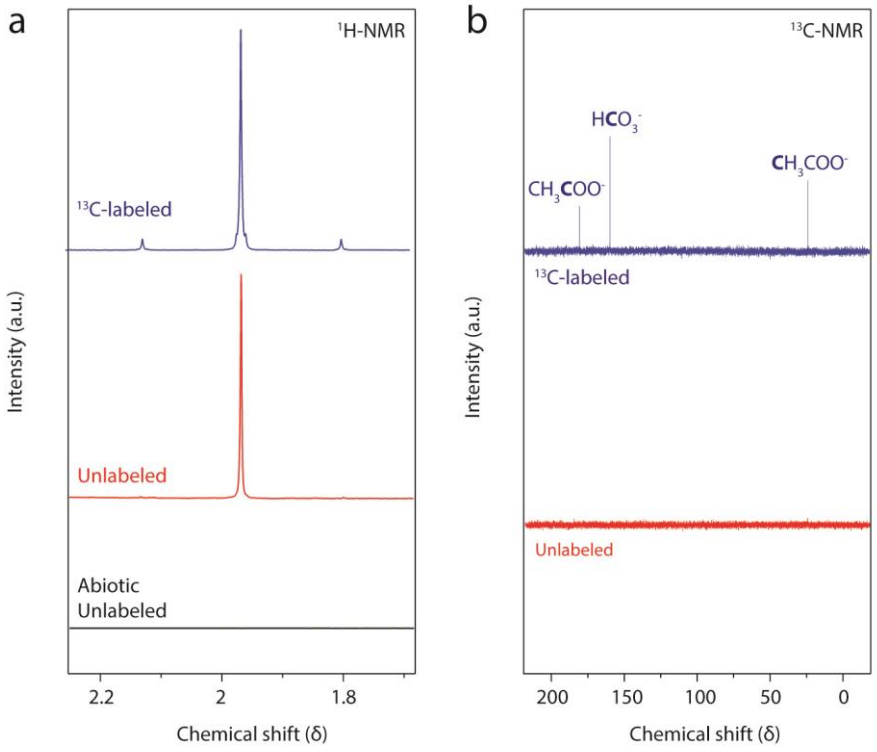

Figure S13. Nuclear magnetic resonance (NMR) characterization of the produced acetate. (a) 1H-NMR spectra of acetate produced with ^{13}C labeled electrolyte (blue) and unlabeled electrolyte (red), and abiotic system (black). For ^{13}C labeled samples, the satellite peaks resulted from $^{1}J_{CH}$ and $^{2}J_{CH}$ coupling. We didn't observe any acetate production in abiotic control experiments. (b) ^{13}C-spectra of acetate produced with ^{13}C labeled electrolyte (blue) and unlabeled electrolyte (red). The ^{13}C signal was observed in bicarbonate and acetate when $NaH^{13}CO_3$ was added to the electrolyte. Since the purged CO_2 gas was not ^{13}C labeled, not all of the produced acetate appeared as ^{13}C labeled.

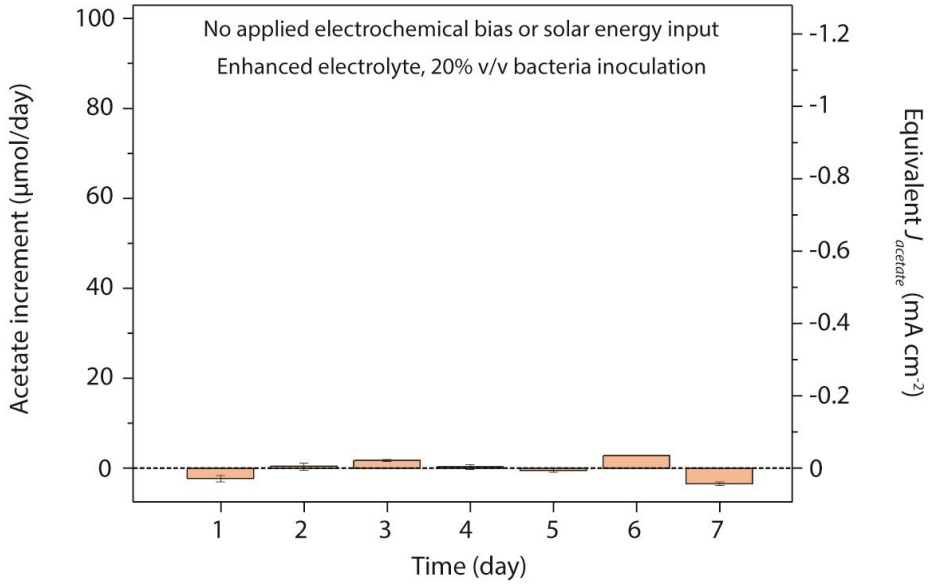

Figure S14. Acetate production under dark or open-circuit condition. The acetate production and equivalent $J_{acetate}$ were negligible when no electrochemical bias or solar energy input was applied.

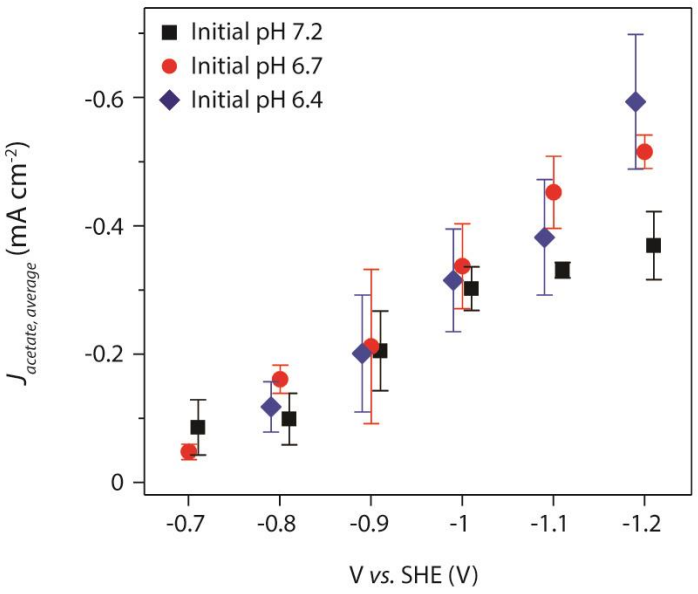

Figure S15. The bias-dependent average CO_2-reducing current density of the optimized electrochemical system. Instead of the $J_{aceatate}$ defined in Fig. 2b, here the $J_{acetate,\ average}$ is calculated based on the acetate production over the whole operating period at each electrochemical potential.

Supplemental References

1. Miguens, F. C., Oliveira, M. L., Marins, R. V., and Lacerda, L. D. (2010). A new protocol to detect light elements in estuarine sediments by X-ray microanalysis (SEM/EDS). Journal of Electron Microscopy *59*, 437-446.
2. Miler, M., and Mirtič, B. (2017). Accuracy and precision of EDS analysis for identification of metal-bearing minerals in polished and rough particle samples. Geologija *56*, 5-18.
3. Sengupta, A. K. (2017). Ion exchange in environmental processes: fundamentals, applications and sustainable technology, 1st ed. Appendix C, (John Wiley&Sons, Inc.), pp. 459-461.